LUND UNIVERSITY

Versatile mobile lidar system for environmental monitoring

Weibring, Petter; Edner, Hans; Svanberg, Sune

Link to publication

Versatile mobile lidar system for environmental monitoring

Petter Weibring, Hans Edner, and Sune Svanberg

A mobile lidar (light detection and ranging) system for environmental monitoring is described. The optical and electronic systems are housed in a truck with a retractable rooftop transmission and receiving mirror, connected to a 40-cm-diameter vertically looking telescope. Two injection-seeded Nd:YAG lasers are employed in connection with an optical parametric oscillator–optical parametric amplification transmitter, allowing deep-UV to mid-IR wavelengths to be generated. Fast switching that employs piezoelectric drivers allows multiwavelength differential absorption lidar for simultaneous measurements of several spectrally overlapping atmospheric species. The system can also be used in an imaging multispectral laser-induced fluorescence mode on solid targets. Advanced LabVIEW computer control and multivariate data processing render the system versatile for a multitude of measuring tasks. We illustrate the monitoring of industrial atmospheric mercury and hydrocarbon emissions, volcanic sulfur dioxide plume mapping, fluorescence lidar probing of seawater, and multispectral fluorescence imaging of the facades of a historical monument. © 2003 Optical Society of America

OCIS codes: 010.3640, 120.0280, 140.3600, 190.4410, 280.1120, 280.1310, 280.1910, 300.2530.

1. Introduction

Environmental conscientiousness is increasing, and the need for effective means of performing environmental monitoring is also stressed. Passive optical techniques employing ambient radiation are convenient and cover large areas, especially when deployed from satellite platforms. However, the complete knowledge of the wavelength distribution utilized in an active system, and especially the possibility of operating with a high spectral resolution that employs laser target illumination sources, adds new possibilities in environmental monitoring with remote-sensing methods. Laser radar, or lidar (light detection and ranging) techniques provide many new possibilities, especially because range-resolved data are obtained.[1] The differential absorption lidar (DIAL) technique is a unique tool for three-dimensional mapping and total flux measurements of gaseous air pollutants,[1–4] and the fluorescence lidar technique is a powerful means for the monitoring of the surface of the sea,[5,6] of terrestrial

vegetation,[7] and of the weathered facades of historical buildings and monuments.[8,9] Whereas the distributed scattering along the laser beam is analyzed at selected wavelengths in atmospheric lidar research, the spectral contents in the fluorescence echo from topographic targets are utilized in the fluorescence lidar approach. The equations describing the phenomena have been discussed, e.g., in Ref. 1.

Our group has been involved in lidar development and applications for almost three decades. Previous mobile lidar systems are described in Refs. 10 and 11 and were employed in numerous scientific and operational monitoring projects. The purpose of the present paper is to describe a new and extremely versatile mobile laser radar system, which is based on all-solid-state laser technology and powerful steering and data handling routines.

The paper is organized as follows. The general construction of the system, including the mobile platform and auxiliary equipment, the optical systems that include the laser transmitter and the receiving telescope, the electronic systems, and, finally, the data collection and handling routines, are described in Section 2. In Section 3 several application examples, including the dominant atmospheric applications but also examples of aquatic and terrestrial monitoring, are given. Finally, a discussion section concludes the paper.
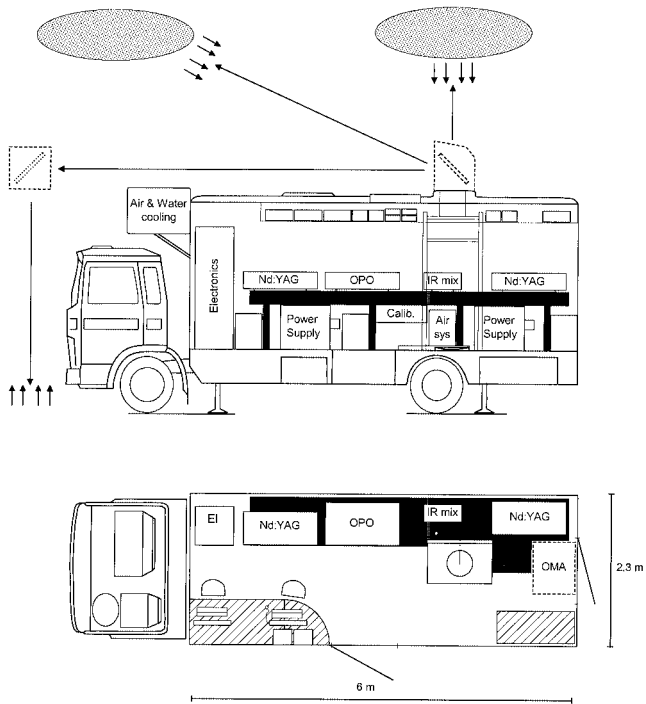
0003-6935/03/183583-12$15.00/0

Fig. 1. Overviews of the mobile lidar system seen from the side and above. They show the standard atmospheric measurement transmission scenario, the arrangement for marine measurements by use of an additional folding mirror, and finally, that for vertical sounding with the transmission dome removed. OPO, optical parametric oscillator; OMA, optical multichannel analyzer.
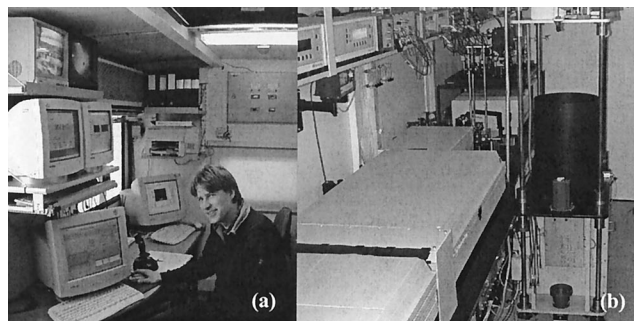

Fig. 2. Two photographs from the bus interior. (a) The control section of the mobile lidar system with the first author. (b) The Nd:YAG laser pumping the OPO unit followed by the IR-mixing unit. Also shown is the vertically looking telescope. In the background, parts of a gas-calibration manifold are shown.

2. System Construction

The new mobile lidar system, consisting of transmitter, receiver, electronics, air-conditioning system, equipment for air cleaning and drying, water cooling, and six computers for control and surveillance, is built on the same vehicle platform that hosted the system described in Ref. 11. The vehicle and the laboratory were fully refurbished and renovated and filled with new equipment. The only essential system remaining partially the same is the vertically looking optical telescope, although the rooftop transmission dome was modified.

A. Lidar System and Auxiliary Equipment

Schematic views of the mobile lidar system are shown from the side and from above in Fig. 1. The truck is a Volvo F610, equipped with a specially constructed laboratory compartment with floor dimensions of 6 m × 2.3 m. Four hydraulic support legs, which can be individually adjusted, are attached to the truck frame to provide platform stabilization. A telescope mast attached to the compartment can hoist an anemometer, which together with a system anemometer, to be placed on a selectable elevated position, can provide wind data for flux estimates. A 45-kVA Diesel-powered electric generator, housed in a trailer, provides the system with power in field experiments. To maintain a stable temperature needed for proper laser system operation, we equipped the laboratory

compartment with an air-conditioning system, consisting of a cooling system and a heating system. It is capable of keeping the air temperature stable to within +/−2 °C in the full outdoor temperature interval of −20° to +30 °C. A closed-circuit water-cooling system for the laser systems was also installed, and a water temperature stability of +/−0.5 °C was achieved by a combination of compressor cooling and an electrical heater under proportional, integral, and differential control.

For shortening beam paths and electric cables, we placed all system components on the right-hand side of the truck, except the computer terminals and monitors, which were installed at the control station on the opposite side. It is possible to monitor and control all functions in the system from the control bench. Two photographs from the bus interior are given in Fig. 2, showing the laser and telescope arrangements and the control station. An overview of the lidar system components and their interconnects is shown in Fig. 3.

B. Optical Systems

1. Laser Transmitter

The transmitter of the lidar system is described in detail in Ref. 12. Its construction allows light pulses to be generated in a very wide wavelength range, from the deep-ultraviolet (UV) to the mid-infrared (MIR) regions, corresponding to 220 nm to approximately 4 μm. The transmitter is a frequency-agile, all-solid-state construction, allowing fast wavelength switching between adjacent shots, delivered at a 20-Hz repetition rate. In contrast to a customary DIAL system operating alternatingly on an on-resonance wavelength and an off-resonance wavelength, the present system is able to make multiwavelength DIAL measurements. In this way it becomes possible to measure several species simultaneously, even if they are partially spectrally overlapping. By the changing of the laser wavelength between every shot, followed by the subsequent signal averaging of the backscattered returns at each
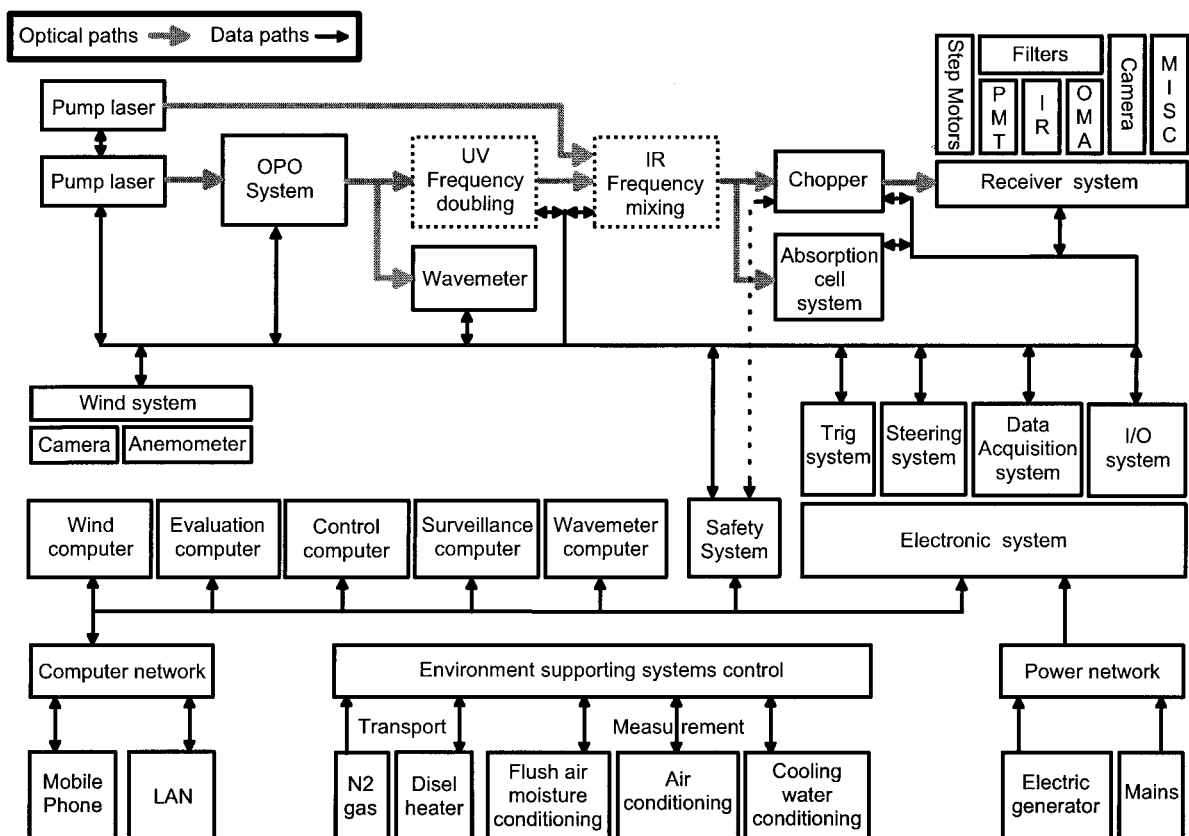
Fig. 3. Overview of the system components and their interconnects and control functions. PMT, photomultiplier tube; LAN, local area network.

selected wavelength, the fluctuations due to the constantly changing atmosphere can be handled.

The transmitter system has four major components: two 20-Hz injection-seeded Nd:YAG lasers (Spectra Physics, Model GCR-290), an optical parametric oscillator (OPO) system modified as discussed below with a Spectra Physics MOPO-730 unit as a base, and an infrared (IR)-mixing system. The OPO operates with β-barium borate crystals, and lithium niobate ($LiNbO_3$) is employed in the nonlinear stages for IR generation. A system for frequency doubling is integrated with the OPO. The two Nd:YAG lasers are the pump sources for the OPO system and the IR-mixing system. The OPO system has a Littman cavity master oscillator generating a narrowband output ($0.07–0.4$ cm^{-1}, with an average ≤ 0.2 cm^{-1}), which is used to seed an unstable cavity power oscillator. The OPO has been modified with actively positioned piezoelectric transducers (Physik Instrumente, Waldbronn, Germany) coupled to the wavelength-tuning elements of the unit as discussed in detail in Ref. 12. Piezoelectric transducers also control the fast phase-matching adjustments of the IR-mixing and doubling crystals. The construction allows a maximum wavelength change of 160 cm^{-1} between subsequent shots, limited by the transducer swaths.

In the first nonlinear crystal (25 mm long) of the IR-mixing system, radiation from the OPO idler beam is mixed through difference-frequency generation with the 1064-nm primary output from one of the Nd:YAG lasers, yielding radiation in the wavelength region of $2.6–4.3$ μm. The generating beams are split off and dumped, and only the generated radiation passes through a second 25-mm-long nonlinear crystal, in which optical parametric amplification with a new 1064-nm beam gives a maximal energy output of 20 mJ in the MIR spectral range.

The doubling stage integrated in the OPO unit produces radiation in the $220–440$-nm wavelength region, by doubling either the signal or the idler from the power oscillator. Pulse powers to as great as 12 mJ can be reached. The wavelength region of 440 nm–1.7 μm, less utilized in environmental monitoring, is covered by the direct OPO generation. The average linewidth of the transmitter is normally better than 0.2 cm^{-1}, and the typical pulse lengths are 3–4 ns.

The laser transmitter system is under full computer control. Status data from the OPO and Nd:YAG laser controllers are transferred to the central system's surveillance computer for logging and evaluation. Overpressurized housings on the different transmitter subsystems protect the optical parts from dust and moisture even in an industrial environment.

Switching from the UV spectral region to the IR spectral region requires some manual adjustments and can be performed in a time span of few minutes.

2. Wavelength Surveillance and Control Systems

To ensure a flawless and consistent operation of the lidar transmitter over wide wavelength ranges, even when the system is deployed in harsh field environments, one needs an elaborate wavelength control system. As central components, it has a wavemeter system (Burleigh, WA-4500) providing absolute wavelength and linewidth data and a system with multiple gas absorption cells to ensure proper tuning and measure the effective absorption of the transmitted radiation.

The application of the Beer–Lambert relation for quantitative gas measurements requires that the linewidth of the radiation be small compared with the absorption lines. Because these linewidths are frequently quite small for the gases of interest and because an OPO system is notorious for occasionally producing some "bad" pulses (i.e., pulses with a considerably larger linewidth or shifted central wavelength or both), unattended operation will necessarily lead to a degrading of the concentration measurement accuracy.

To deal with this problem, we used a surveillance system to monitor the transmitter performance in real time on a shot-to-shot basis. The laser shots are categorized in the wavemeter on the basis of the fringe patterns from two etalons with different resolutions. A Gaussian is fitted to the measured emission pattern, and the half-width of the Gaussian is considered to be the linewidth of the shot. To get absolute wavelength values, we compared the etalon patterns with patterns from a stable He–Ne reference laser. The lidar return signals are then stored in different preselected bins according to the linewidth of the laser shot fired. During the data evaluation process, a concentration look-up table for varying linewidth and wavelength could be used to calculate the correct concentration based on each subset of data.

The wavemeter with its etalon system is fed by a split-off beam from the direct OPO output. The OPO performance is transferred through the frequency-doubling or IR-mixing system although frequency shifted, and thus the same surveillance is available when it operates in the UV and IR regions.

As an independent and mainly analog modality, the laser transmitter surveillance system also includes a cell reference system, which is described in more detail in Ref. 13. Absorption cells, mounted on a turret and containing gases of known concentration, can be rotated into a split-off portion of the output beam from the transmitter system. The partially absorbed beam and a separate reference beam are monitored by individual detectors, allowing absorption spectroscopy to be performed in parallel with the atmospheric measurements. In this way, shot-to-shot comparisons of the effective absorption cross section can be performed, allowing the possibility of compensating for moderate deviations in both wavelength and linewidth. Basically, external unknown concentrations are measured in terms of internal, well-known concentrations. Data are fed into the control computer and are integrated in the evaluation procedure. By combining data from the wavemeter system and the gas absorption cell system during runs, during which the laser system is producing shots of varying characteristics, it is possible in principle to generate the look-up tables used for an optimal external gas concentration measurement by use of almost all the laser pulses transmitted.

3. Transmitting and Receiving Telescope

The lidar receiver system consists of a vertically looking, 40-cm-diameter Newtonian telescope with a focal length of 1 m and a transmission dome, which can be hoisted through a port in the laboratory roof. The arrangements are shown in Fig. 1. A folding transmission mirror of size 70 cm × 40 cm is mounted inside the dome, which can be rotated 360 deg with a stepper motor, yielding an angular resolution of 0.0035 deg. The folding mirror is also controlled by a stepper motor, yielding a resolution of 0.011 deg and a vertical beam-steering interval of −10 to 55 deg. A large quartz window seals off the transmission dome. Also, to achieve a well-defined overlap between the outgoing laser beam and the field of view of the receiver telescope for close-range measurements, we have the laser beam transmitted from a Galilean quartz lens beam expander mounted coaxially with the vertically looking telescope. The beam expander allows control of the divergence of the transmitting beam and also reduces the power load on the first surface-aluminized steering mirror. A totally reflecting 90-deg prism, which can be tilted under computer control to achieve easy overlap between the transmission and the receiving lobes, is used to inject the laser beam into the expander.

A tilted polished metal mirror with a central aperture, which can be further narrowed by an iris to define the telescope field of view, is used to reflect light into a television camera, providing a sharp image of the target area. The lidar laser beam is pointing where the black spot due to the opening occurs on the television screen; one can simply steer the beam to selected target directions by using a joystick; which controls the transmission mirror stepper motors. Backscattered radiation passing the central aperture then enters the detector compartment, in which different detectors can be selected by use of a beam-splitting system. Dichroics and bandpass filters can be introduced in the beam. Two photomultipliers (PMTs), as well as an IR detector, can be attached. Alternatively, a circular multifiber arrangement can be introduced in the telescope focus, with subsequent transmission of laser-induced fluorescence from a solid target to the entrance slit of a time-gated optical multichannel system (OMA). The individual fibers are then linearly rearranged to match the spectrometer slit. The OMA system consists of an optical spectrometer, an image intensifier gateable down to less than 10 ns, and a high-quality CCD detector on which the spectra are captured. The data are appropriately binned on the detector, and an effective

resolution of approximately 10 nm is achieved. The fluorescence measurement mode is more closely described in Ref. 14.

The main PMT (Thorn-EMI, 9816QA), utilized in UV–visible atmospheric DIAL is reconstructed to allow a ramped voltage to be applied to the dynode chain for a set time period and then to remain constant at the final value. In this way the dynamic range of the PMT is improved, and the risk of obtaining signal-induced background originating from the dome window reflection or near-field backscattering is reduced.

Sometimes, e.g., in ship-based volcanic plume monitoring, it is desirable to perform vertical lidar sounding with minimal loss of signal. Then the transmission dome can be dismounted easily and moved aside on the laboratory roof. The transmission dome quartz window can then instead be mounted at an angle for weather protection of the telescope. To further reduce the risk of a signal-induced background in long-range measurements with minute atmospheric returns, one can use an off-axis vertical transmission arrangement by employing a rooftop hole, taken up 45 cm beside the telescope optical axis.

The new lidar system is versatile and can also be used in quay-based or shipborne aquatic monitoring campaigns for depth-resolved laser-induced fluorescence or Raman measurements. Then the laser beam is directed from the transmission dome toward the front of the truck, at which a second folding mirror is placed to direct the beam vertically down toward the water surface as indicated in Fig. 1. Backscattered light is retracing the path to the receiving telescope and is directed to the gated OMA system. This measuring mode is described more closely in Ref. 15.

C. Electronic Systems and Computers

The mobile lidar system contains extensive electronics. The power supplies for the Nd:YAG lasers are placed under the vibrationally isolated bench carrying the laser heads. The control units for the Nd:YAG lasers, the OPO and frequency-doubling system, a delay unit, and the temperature controllers of the ovens containing the IR-mixing crystals are placed on a shelf above the transmitter system for easy access. All essential functions of the units can be accessed by the control computer. The delay unit (Stanford Research Systems, DG535) has a key function because it controls the timing of all signals, such as triggering of lasers, piezostack movements, wavemeter, signal-integrating unit, PMT modulation, laser intensity detectors, data logging, and the OMA system.

All other electronics are housed in a rack cabinet, placed in the corner of the laboratory compartment. It contains a switchboard, the transient digitizer unit, the PMT high-voltage and modulation unit, a signal-integrating unit, a power unit, and an operational safety unit. Finally, the control, evaluation, wavemeter, and surveillance computers are placed in the cabinet.

The switchboard unit handles all signals entering or leaving the control computer. The digitizer unit (Licel) consists of two 20-MHz, 12-bit analog digitizers running in parallel with two 250-MHz photon counters, which yield an improved signal retrieval for large ranges, where the signal return consists of separable photons. The signal-integrating unit handles the detector signals from the reference cell system and from the IR-mixing unit. The power unit contains the electronics used to drive and control stepper motors, servo motors, the retractable dome window weather-protection cover, the chopper that interrupts the laser beam for background signal collection, and the OMA system interface.

The operational safety unit ensures that lidar measurements can be performed with maximized safety for the public, providing conditional automatic shutdown of the laser beam transmission into the atmosphere. As mentioned above, the system's optical design allows a television camera to clearly indicate the current position of the laser beam. An additional television camera, placed in the transmission dome next to the folding mirror, produces a view of the target area and its surroundings. The cameras, in conjunction with an analog system comprising potentiometers that are attached to the dome and mirror-turning mechanics and providing proportional voltages to be compared with hand-set potentiometer-controlled voltages, allow a safe shooting window, defined horizontally and vertically, to be set. If the steering mirror, owing to malfunction of the computer, tries to drive the laser beam outside the set window, an analog interlock system inhibits the movements. The outgoing beam can be blocked by the mechanical chopper, not only by the computer programs but also by two emergency buttons placed inside the bus or by a remote wire-connected button activated by an outdoor observer. It should be noted that beam transmission from the rooftop dome 4 m above the street level is a key safety aspect and also that the eye security range for the most used wavelength ranges (below 400 nm and above 1.4 μm) typically are only tens of meters.

The data control and processing system comprises five computers: control, evaluation, wavemeter, surveillance, and wind computers. When measurements with laser-induced fluorescence are performed, an OMA control computer is also utilized. The computers are connected in a local Ethernet through a hub in the laboratory compartment. The network can be connected to other Ethernet networks through a BNC, a twisted pair, or a mobile phone connection. All the programs running the system use LabVIEW as the platform. All system functions are accessed through a menu system and are controlled by a mouse or joystick.

During a measurement the control computer, via six plug-in boards, controls the angular settings of the dome, the transmitter wavelength, and the acquiring of data from the transient digitizer or the OMA computer. It also handles some data evaluation. However, the essential data processing is per-

formed by the evaluation computer, which then displays the concentration measurement results on line and combines wind and concentration measurements to fluxes. Because lidar data taking is possible without running the evaluation computer, it can be used for evaluation of other measurements while new data is taken.

The wavemeter computer handles data regarding wavelength and wavelength purity as discussed above and provides input to the surveillance computer, which in turn informs the control computer of the spectral properties of individual shots. The control computer then stores the measured data accordingly.

The wind computer calculates the wind speed and informs the control computer of the result at the end of a particular measurement direction. This is done by application of a power law for vertical wind profiles, [16] with input data from two anemometers at different heights. Alternatively, the wind speed pertaining to a visible plume can be evaluated by cross correlation of data from the surveillance video camera as described in Ref. 17.

D. Data Collection and Handling

All programs used in the lidar system operation and data handling are stored on the control computer. They can also be accessed from the other computers but be run only by the units, which have the required hardware for the specific task. The operator interacts with the software, and thus with the full lidar system, through more or less self-explanatory pull-down menus. Starting from a main menu, it is possible to reach all functions of the system to perform a measurement. The operation can logically be divided into two steps: (1) measurement definition and (2) data evaluation and presentation following the measurements defined in the first step.

1. Measurement Definition

When the system has been positioned at the proper location and is made ready to take data, the measurement task has to be defined. Three aspects must be covered in the definition of a measurement: a wavelength definition, a spatial definition, and a sequential definition.

The *wavelength definition* is largely dependent on the gas or gas mixture to be studied. The transmission wavelengths between which the laser system switches between shots should be selected in an optimum way. On the basis of previous experience, they can be entered digitally or be loaded from a file. Alternatively, the absorption spectra of a number of gases, selected from a large database, can be displayed, and cursors can be moved to the wavelengths at which the laser should fire. A particular example is shown in Fig. 4, showing the cases of methane, ethane, and propane, with markers indicating seven selected wavelengths for a multiwavelength DIAL measurement. As described in Ref. 18, the selection can be optimized by use of multivariate techniques to orthogonalize the different molecular
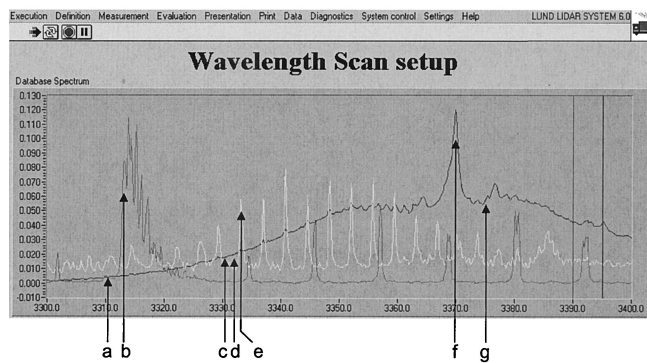

Fig. 4. Screen dump from the wavelength definition menu showing multiwavelength selection for a mixture of methane, ethane, and propane. Seven wavelengths, indicated by a–g, are marked.

constituents as much as possible with a set number of transmission wavelengths; one could select as many as 50. However, it should be noted that the requirement of a minimum signal-to-noise ratio in the signal averaging, in conjunction with time restraints relating to a varying-emission situation, frequently reduces the number of wavelengths to well below 10.

The *spatial definition*, i.e., the selection of the beam directions to be used for the particular task, can vary from a fanlike vertical scan pertinent to flux measurements downwind from a plant, a horizontal panorama, to a matrix scan used in fluorescence imaging. The joystick-operated beam, aimed in directions defined with the boresight video camera as described above, allows easy definition of preferred spatial scan files, which can be stored and later recalled. Actual measurements are made by combining different wavelength and spatial definitions in a *sequence definition*.

With all the parameters set, it is possible to initiate the measurement. An example of data collected during a measurement of atmospheric emission from a chlor-alkali plant at Rosignano Solvay in Italy is shown in Fig. 5. In the lower right part of the screen printout, particular wavelength and spatial definition files have been selected, forming a sequence definition. Raw averaged on-and off-resonance curves are shown to the left together with the ratio (DIAL) curve and the evaluated range-resolved concentration.

2. Evaluation and Presentation

Classical two-wavelength DIAL evaluation or partial least-squares regression methods for the multiple-species, multiple-wavelength situation can be used in atmospheric applications. Similarly, in laser-induced fluorescence measurements, a simple intensity ratio formation for selected wavelengths or a full multivariate (partial least squares or principal component analysis) analysis[19,20] of the OMA spectra can be employed for delineating target areas of different types.

Data recorded can undergo a primary processing in which, e.g., background is subtracted, filtering func-
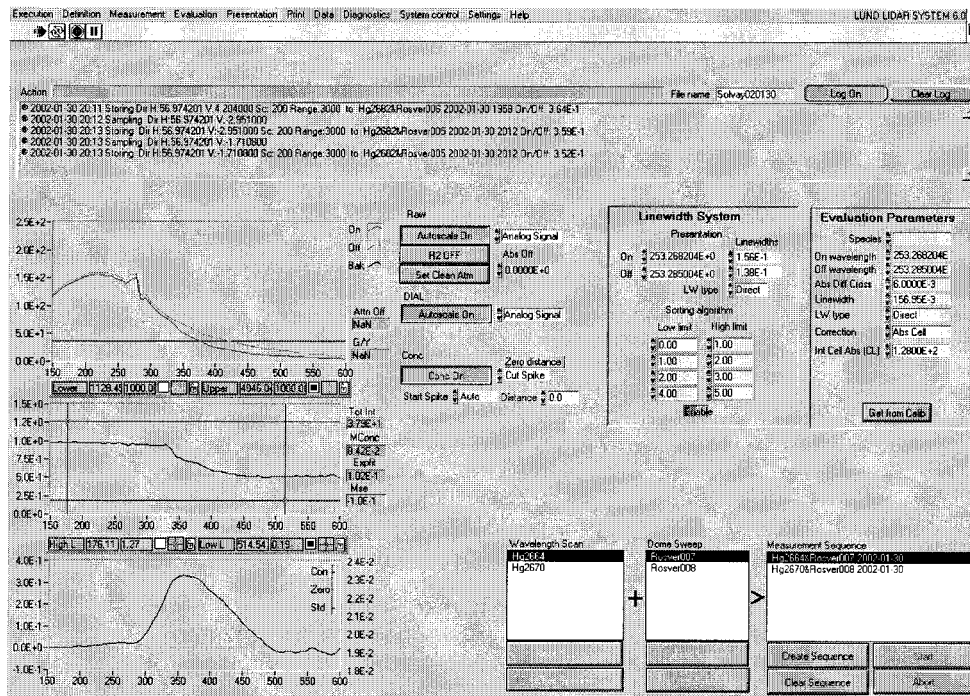
Fig. 5.   Screen dump of the measurement menu during an atomic mercury run.   To the left, the on-and off-resonance averaged lidar curves are shown.   Below, the on/off ratio curve is shown, and, at the bottom, the evaluated concentration curve, displays a plume at approximately 350 m in distance.   To the lower right, a measurement definition with wavelength and spatial components is shown.

tions are applied, and the $1/R^2$ signal falloff is compensated for. An evaluation functions library includes routines for concentration evaluation such as direct differentiation or integration of the DIAL curve and also more advanced methods such as locally weighted regression and partial least-squares regression.[21,22]

The outcome of a whole measurement can be viewed in the presentation menu. It is possible to produce two-dimensional concentration plots together with the vertical and horizontal integrated profiles. Accuracy profiles can also be calculated. By merging wind data as discussed above, one can evaluate the total flux. By combinination of many sequential plume cross sections, a movie that shows the time evolution of the emissions can be made.

3. Lidar Applications

A. Range-Resolved Backscattering for Atmospheric Monitoring

The primary applications of the lidar system described in this paper are range-resolved measurements of air-pollutant concentrations and the evaluation of the total gas flux from the source under study. When no or little species interference occurs, it is possible to perform DIAL measurements with the conventional two-wavelength approach, transmitting subsequent laser shots on an on-absorption wavelength and an off-absorption wavelength. We will illustrate this measurement mode by two examples, both utilizing UV wavelengths but operating on different spatial scales: atomic mercury emission from

a chlor-alkali plant and sulfur dioxide emission from the Italian volcano Mount Etna.

Hydrocarbon mixtures with overlapping spectra in the MIR spectral region constitute an example for which the full capability of multiwavelength DIAL of the new lidar system is utilized. We demonstrate such measurements at a hydrocarbon test facility, in which controlled releases of hydrocarbon mixtures can be made.

1. Utraviolet Dual-Wavelength Differential Absorption Lidar

Mercury is the only pollutant that is present in the atmosphere in atomic form. Background concentrations are of the order of 1 part per 10^9, and, because the whole transition oscillator strength is aggregated in a single line (apart from isotopic shifts and hyperfine structure) at approximately 254 nm rather than distributed on thousands of vibrational–rotational transitions in a molecule, even such low concentrations can be assessed. We have previously measured mercury emissions at chlor-alkali plants and in geothermal fields but used a dye-laser transmitter.[23,24]   Figure 6 shows the result of a vertical lidar scan through the mercury emission plume downwind from an Italian chlor-alkali plant, as obtained with the new lidar system.   In total, 4000 laser shots fired during approximately 4 min were used to produce the data. The OPO system generated close-lying green output wavelengths, which were frequency doubled to the matching on-and off-resonance wavelengths of mercury.   The corresponding lidar returns were ex-
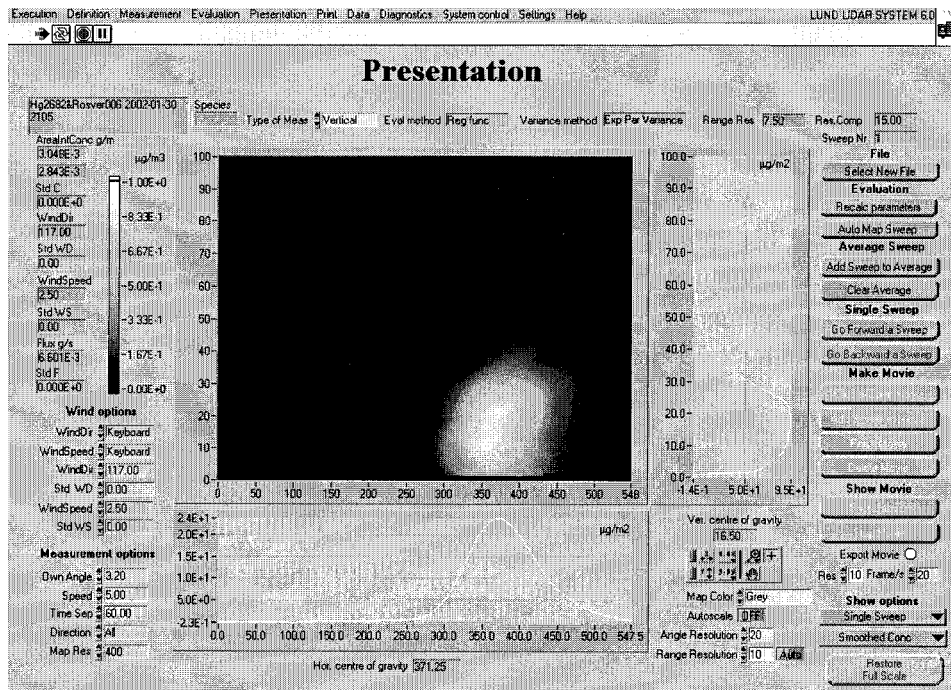
Fig. 6.   Atomic mercury concentration distribution retrieved in a vertical scan downwind from the Rosignano Solvay chlor-alkali plant in Italy.   A screen dump from the presentation menu is shown, in which the image is built up by data of the type shown in Fig. 5.

emplified in Fig. 5.   The graph in Fig. 6 shows the concentration distribution (grams per cubic meter) and the horizontally and vertically integrated values $(g/m^3 \times m = g/m^2)$.   If the surface-integrated value $(g/m^3 \times m^2 = g/m)$ is multiplied with the perpendicular wind component (meters per second), the total flux $(g/m \times m/s = g/s)$ is obtained.   As indicated in Fig. 6, the total flux of atomic mercury downwind from the electrolytic cell house in which the vertical scan was made was 6.6×10^{-3} g/s.   The calibration can be performed by insertion of an air-filled cell of known thickness that contains a drop of mercury in the gas-calibration unit.   By accurate measurement of the temperature, the vapor density can be calculated.   Further atomic mercury flux measurements with the new lidar system are reported in Ref. 25.

Sulfur dioxide is a main pollutant emitted when fossil fuels are burned or sulfide ores are roasted. Much lidar research has been performed by the mapping of such emissions from industries.   The normal on-and off-resonance wavelengths for sulfur dioxide monitoring are 300.02 and 299.30 nm, respectively. We have utilized the new lidar system from the aft deck of the Italian research vessel *Urania* to monitor the total sulfur dioxide emission from Mount Etna. The ship performed linear transects under the plume with the system firing vertically in the off-axis vertical transmission mode with the transmission dome removed.   A pulsed dye laser was used in these particular measurements.   On-and off-resonance lidar return signals averaging 300 laser shots for each wavelength are shown in Fig. 7(a).   By evaluation of data of this kind all along the track, the volcanic plume concentration profile can be produced as

shown in Fig. 7(b).   The plume height reflects the volcano's summit height of 3340 m, and a strong and typical stratification is shown.   By combination with meteorological wind data, a total flux of approxi-
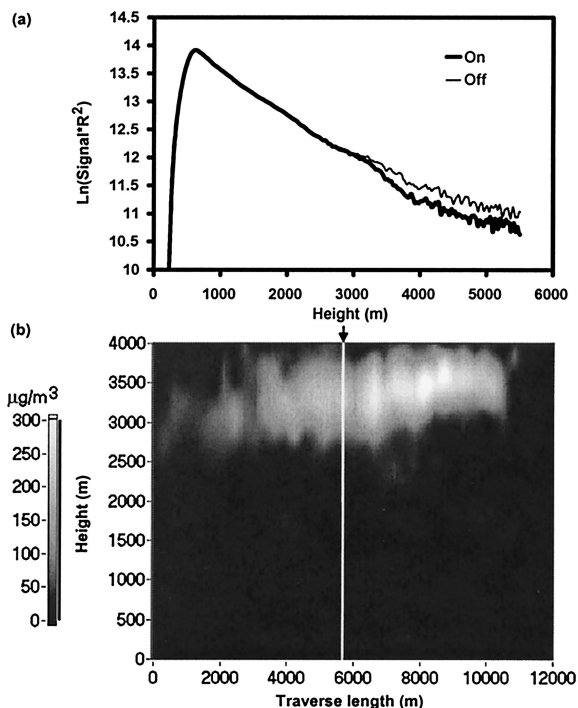

Fig. 7.   (a) On- and off-resonance averaged lidar returns in vertical measurements under the volcanic plume of Mount Etna.   (b) Sulfur dioxide distribution from Mount Etna as recorded with the lidar system firing vertically in a ship during a full underpass of the plume.
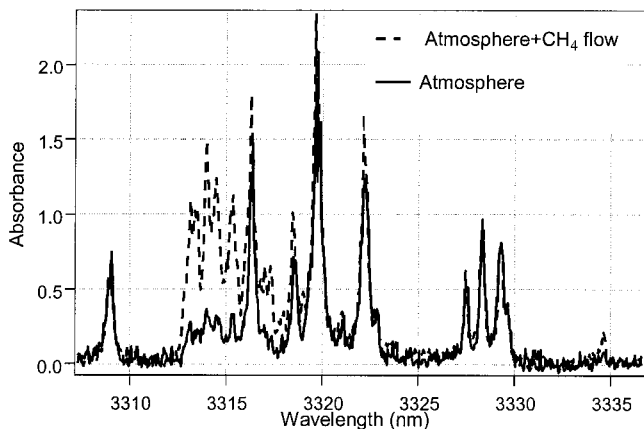
Fig. 8. Remote lidar recording of methane streaming through a 0.4-m-diameter, 3-m-long open-ended tube positioned 60 m from the lidar system. A topographic target was placed behind the tube, and the transmitter was continuously tuned to produce a full spectrum. The signal remaining when the gas flow is shut off corresponds to the ambient air concentration of methane and the atmospheric concentration of water vapor.

mately 75 tonnes/h is estimated. Volcanic plume monitoring with the new lidar system is further discussed in Ref. 26.

2. Mid-Infrared Multiwavelength Differential Absorption Lidar

The new lidar system was tested in hydrocarbon measurements around 3.4 μm. We performed these measurements at a specially constructed lidar testing facility, at which well-defined amounts of different hydrocarbons could be admixed to a controlled airflow, conducted to expand from the center toward the open end of a 0.4-m-diameter tube of a total length of 3 m. Data for methane are shown in Fig. 8. A topographic target was arranged on the lateral end of the tube, and the lidar echo from the hard target was integrated and displayed as the laser was tuned through the absorption features of methane around 3.4 μm. The signal remaining when the gas flow is shut off corresponds to the ambient air concentration of methane, approximately 2 parts per 10^6.

Range-resolved DIAL measurements on hydrocarbons were also performed at the same test facility. Averaged (200 shots) lidar returns at 3.4 μm are shown in Fig. 9(a), illustrating the range capability of the system. In Fig 9(b) the ratio curve for on-and off-resonance wavelengths for methane, corresponding to the wavelengths b and a in Fig. 4, are shown. The clear step at approximately 60 m corresponds to a localized plume of methane, flowed through the test tubing. The slope in the ratio curve before as well as behind the step corresponds to the ambient atmospheric concentration of methane. In Fig. 9(c) a ratio curve for on-and off-resonance wavelengths of ethane, corresponding to positions e and d in Fig. 4, is shown; a corresponding curve for propane (positions f and g in Fig. 4) is shown in Fig. 9(d); and, finally, a ratio curve for two off-resonance wavelengths (c and

d in Fig. 4) is shown in Fig. 9(e). For each of the two wavelengths involved in the ratio curves shown, data from 200 laser shots were averaged. The laser pulses had a typical energy of 8–10 mJ. The data clearly show the multigas capability of the system. Test experiments with as many as 60 transmission wavelengths were performed, and methane, ethane, propane, and butane could be measured simultaneously. Wavelength selection and data evaluation were performed according to multivariate routines. Data of this kind are discussed in more detail in Ref. 18.

B. Laser-Induced Fluorescence in Solids and Liquids

As described earlier, the new mobile lidar system is well adapted for laser-induced fluorescence measurements on solid and liquid targets. For excitation, the frequency-tripled output at 355 nm from one of the Nd:YAG lasers is particularly straightforward. High pulse energies to as great as hundreds of millijoles can be obtained, but normally the energy is limited to tens of millijoules. With the availability of a wide variety of excitation wavelengths from the OPO transmitter, additional discriminating power in fluorescence analysis of, e.g., different types of vegetation or different types of surface material in historical buildings is obtained.

1. Aquatic Applications

The most common application of laser systems in marine monitoring is for bathymetry, by which the elastic echo for the sea floor is detected. Blue-green radiation penetrates water best, and a depth range down to tens of meters can be achieved. If the elastic scattering is suppressed, the laser-induced fluorescence can instead be detected. Major chromophores in water are dissolved organic matter (DOM), giving rise to a broad fluorescence light distribution in the blue-green region, and chlorophyll from microscopic algae (plankton), featuring a main peak around 685 nm. In addition, a strong sharp signal due to the O–H-stretch Raman scattering in the water molecules occurs with a characteristic shift of 3400 cm^{-1}, corresponding to a spectral position of 404 nm for 355-nm excitation. By normalization of the chlorophyll and the DOM signal to the freestanding water Raman signal, effects due to observational geometry, light-penetration properties, etc., are eliminated.

Examples of water fluorescence data are shown in Fig. 10. The data were recorded during a shipborne measurement campaign around Sicily when atmospheric as well as marine experiments were performed.[15] As described in Subsection 2.B.3, 355-nm pulses were transmitted horizontally from the dome over the compartment roof to hit a 45-deg mirror placed outside the railing of the ship. Water emission was collected in a retrograde beam path and was dispersed and recorded in a gated and intensified OMA system. The strong elastic scattering from the water surface and column was suppressed with a colored glass filter. In part (a) of the figure the sig-
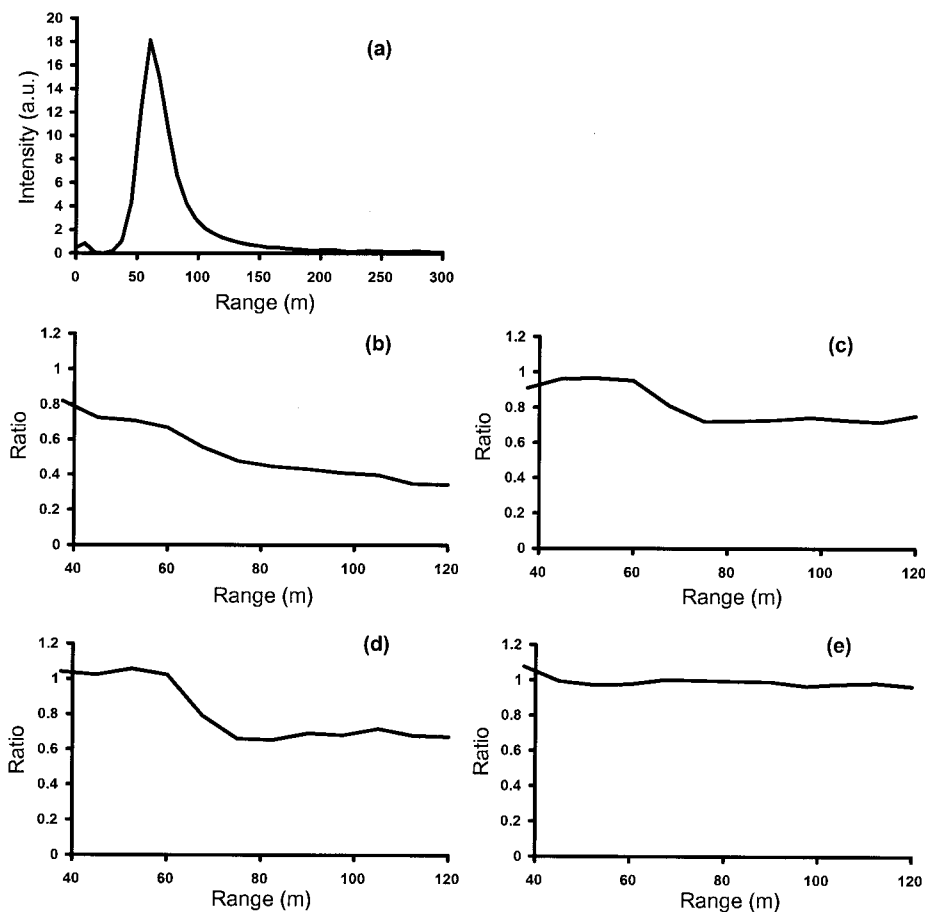
Fig. 9. (a) Range-resolved atmospheric backscattering lidar curve at 3.4 μm showing a range of approximately 200 m. (b)–(e) Partial data from a multigas, multiwavelength DIAL measurement involving 60 different transmission wavelengths. (b) Curve corresponds to methane, formed by division of an on-resonance wavelength curve by an off-resonance wavelength curve (wavelength positions b and a in Fig. 4). (c) The characteristic DIAL curve step is shown for ethane, corresponding to divided curves at wavelengths e and d in Fig. 4. (d) Corresponding data for propane are shown (wavelengths f and g in Fig. 4), and (e) transmission of two off-resonance wavelengths (c and d in Fig. 4) results in a ratio value of 1.0 and no trace of the flow-cell arrangement.

nal evolution when the ship enters the Italian harbor of Civitavecchia is shown with increasing DOM concentrations. Depth-resolved curves are shown in part(b). A 40-ns gate for the image intensifier could be activated at different delays, resulting in fluorescence curves pertaining to water slices at approximately 4-m-thick depth intervals. Data from two depths are shown. It would be of particular interest to gate in the fluorescence signal from the bottom vegetation, but, owing to the constrictions on shallow-water passage of the research vessel, we were not able to reach the bottom signal. With the system mounted on a smaller vessel or barge, *in situ* monitoring of, e.g., *Posidonia oceanica*, which is an important environmental bioindicator, would be possible.

2. Terrestrial Applications

If an UV laser beam is instead terminated on a solid target such as vegetation or a building wall, the induced fluorescence can be picked up by the receiving telescope. As described in Subsection 2.B.3 the fluorescence from the illuminated spot is then imaged on the entrance of an optical fiber assembly and con-

ducted to the entrance slit of a spectrometer. An image intensifier in front of the CCD detector is gated to match the arrival time of the signal. The beam is swept row by row until a full matrix covering a certain area at the target is covered. As an example, a 8 m × 8 m area of the facade of the cathedral in Parma, Italy, is shown in the lower part of Fig. 11. Part of the stone area had been treated with a restoration solution binding the surface and reducing decay. Excitation of 355 nm was performed from a distance of approximately of 80 m, and a laser spot size at the target of approximately 6 cm was used. A processed image in which the fluorescence intensity ratio image $I(400 \text{ nm})/I(445 \text{ nm})$ is displayed clearly demarcates the treated areas. The origin of the demarcation is evident from the inserted spectra shown for treated areas and normal stone. Also included in Fig. 11 is a different measurement of the upper part of the baptistery next to the cathedral. Here the $I(685 \text{ nm})/I(645 \text{ nm})$ ratio is displayed, sensitive to chlorophyll and demarcating areas of biodeteriogen invasion as can easily be understood from the inserted spectra for invaded and nonaffected stone.
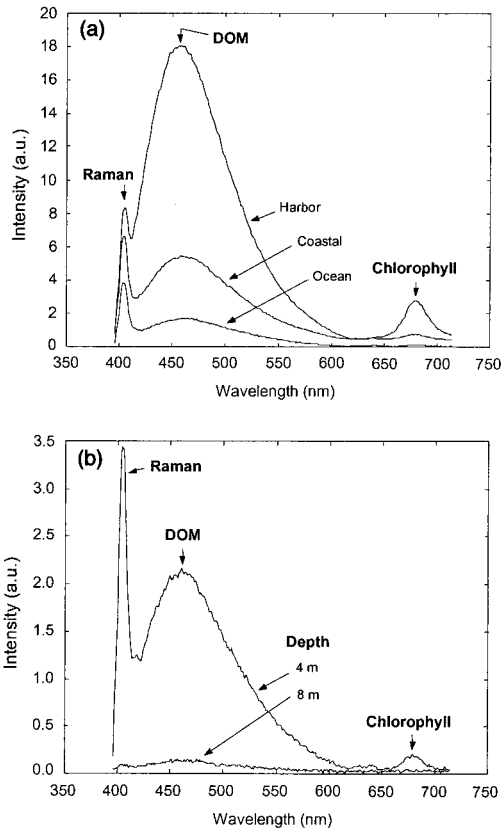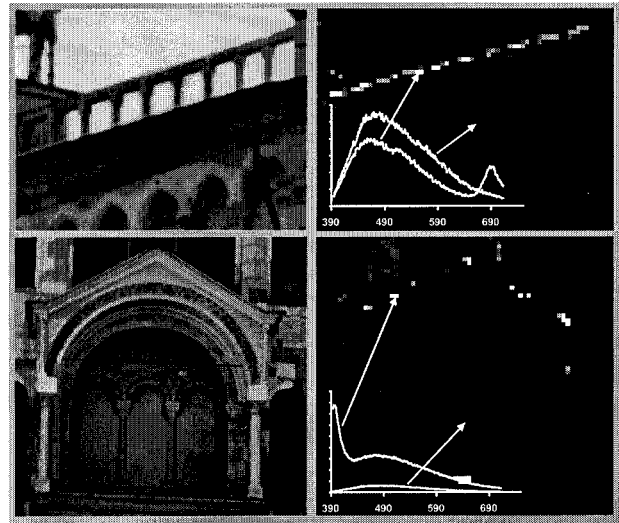
Fig. 11. (bottom) Photograph and fluorescence image from a portion of the Parma cathedral, showing areas that had been subject to surface-protection treatments. Excitation of 355 nm was used, and the ratio intensity $I(400 \text{ nm})/I(445 \text{ nm})$ is displayed. (top) Photograph and fluorescence image of the upper part of the baptistery in Parma showing areas with algae coverage. The intensity ratio $I(685 \text{ nm})/I(645 \text{ nm})$ is displayed. Individual spectra are inserted to indicate the spectral basis of the discrimination. The total time for each image recording was approximately 2 h.

Fig. 10. Fluorescence data obtained for Mediterranean water during a measurement campaign on board the Italian research vessel *Urania*. (a) The data shows increasing levels of DOM as the ship is entering the port of Civitavecchia. The recordings correspond to the integrated fluorescence intensity of the water column. (b) Two depth-resolved fluorescence curves showing the signal integrated over a 4-m column centered at approximately 4-and 8-m depths.

More detailed information of fluorescence imaging at historical monuments is given in Refs. 9 and 27.

To demarcate different types of stone is more subtle, and here the use of a variety of excitation wavelengths is useful as is illustrated in Fig. 12. An arrangement of different Italian marble slabs as shown in the photograph was studied from a distance of approximately 60 m. The tunable OPO laser system was used to generate 250-, 280-, 300-, and 399-nm radiation, the target was scanned for each wavelength; and for each measurement point the full fluorescence spectrum was recorded. Spectra for different types of marble are shown in the lower part of the figure. By employing multivariate analysis methods, it was possible to combine the information obtained at the different excitation wavelengths to uniquely characterize five different stone types and identify the areas of the same spectral characteristics, pertaining to individual marble slabs.

4. Discussion

As illustrated in this paper and to a fuller extent in Ref. 28, the new mobile laser radar system can perform a multitude of advanced remote-sensing tasks, ranging from air-pollutant mapping in wide wavelength ranges to aquatic and terrestrial monitoring by employment of laser-induced fluorescence. In that it is truly mobile and has all support systems
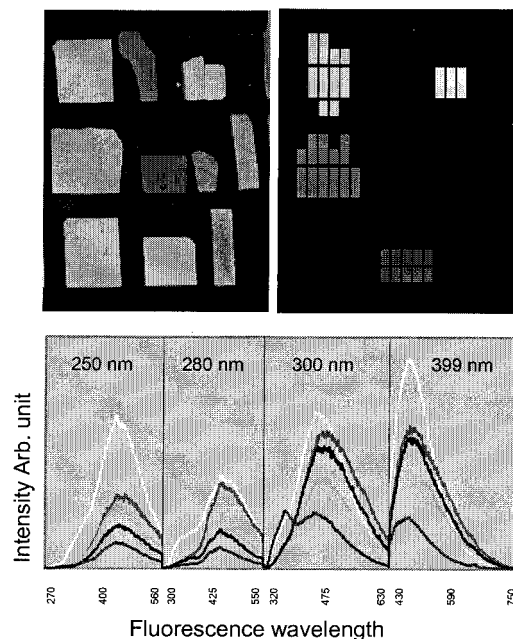

Fig. 12. (bottom) Fluorescence spectra recorded from an arrangement of Italian marble slabs, by use of four excitation wavelengths. The different responses of different materials is illustrated. By use of multivariate analysis, the spectral data was combined to yield a consistent stone identification for the areas indicated in the upper right part of the figures.

including a powerful electric generator, integrated, it provides efficient environmental monitoring almost anywhere and for many different tasks. It can thus provide an important service in elucidating our environment and yield information otherwise extremely difficult to obtain. It also provides an important test bed for developing airborne or satellite-based sensors.

References

1. R. M. Measures, *Laser Remote Sensing* (Wiley-Interscience, New York, 1984).
2. S. Svanberg, "Differential absorption lidar (DIAL), " in *Air Monitoring by Spectroscopic Techniques*, M. Sigrist, ed. (Wiley, New York, 1994).
3. R. A. Robinson, P. T. Woods, and M. J. T. Milton, "DIAL measurements for air pollution and fugative-loss monitoring, " in *Air Pollution and Visibility Measurements*, Proc. SPIE **2506,** 140–149 (1995).
4. L. Fiorani, B. Calpini, L. Jaquet, H. van den Bergh, and E. Durieux, "A combined determination of wind velocities and ozone concentrations for a first measurement of ozone fluxes with a DIAL instrument during the MEDCAPHOT-TRACE campaign, " Atmos. Environ. **32,** 2151–2159 (1998).
5. F. E. Hoge, C. W. Wright, R. N. Swift, and J. K. Yungel, "Airborne laser-induced oceanic chlorophyll fluorescence: solar-induced quenching corrections by use of concurrent downwelling irradiance measurements, " Appl. Opt. **87,** 3222–3226 (1998).
6. L. Fiorani, R. Barbini, F. Colao, R. Fantoni, and R. Palucci, "Comparison between satellite and laser remote sensing of the Southern Ocean, " J. Comput. Technol. **7,** 110–120 (2002).
7. S. Svanberg, "Fluorescence lidar monitoring of vegetation status, " Phys. Scr. **T58,** 79–85 (1995).
8. V. Raimondi, G. Cecchi, L. Pantani, and R. Chiari, "Fluorescence lidar monitoring of historical buildings, " Appl. Opt. **37,** 1089–1098 (1998).
9. P. Weibring, Th. Johansson, H. Edner, S. Svanberg, B. Sundnér, V. Raimondi, G. Cecchi, and L. Pantani, "Fluorescence lidar imaging of historical monuments, " Appl. Opt. **40,** 6111–6120 (2001).
10. K. Fredriksson, B. Galle, K. Nyström, and S. Svanberg, "Mobile lidar system for environmental probing, " Appl. Opt. **20,** 4181–4185 (1981).
11. H. Edner, K. Fredriksson, A. Sunesson, S. Svanberg, L. Unéus, and W. Wendt, "Mobile remote sensing system for atmospheric monitoring, " Appl. Opt. **26,** 4330–4338 (1987).
12. P. Weibring, J. N. Smith, H. Edner, and S. Svanberg, "Development and testing of a frequency-agile optical parametric oscillator system for differential absorption lidar," Rev. Sci. Instrum., submitted for publication.
13. F. Mellegård, "Development and construction of an automatic calibration unit for a differential absorption lidar system, " diploma paper, *Lund Reports on Atomic Physics*, LRAP 264 (Lund Institute of Technology, Lund, Sweden, 2000).
14. H. Edner, J. Johansson, S. Svanberg, and E. Wallinder, "Fluorescence lidar multicolor imaging of vegetation," Appl. Opt. **33,** 2471–2479 (1994).
15. I. Mochi, G. Cecchi, L. Pantani, Th. Johansson, P. Weibring, H. Edner, and S. Svanberg, "Probing the marine environment with fluorescence lidars—comparison of three fluorosensors in a field campaign, " CNR Scientific Report RR/OST/01.03 (Consiglio Nazionale delle Ricerche, Rome, Italy, 2003).
16. S. A. Hsu, E. A. Meindl, and G. B. Gilhousen, "Determining the power-law wind-profile exponent under near-stability conditions at sea, " Appl. Metrol. **33,** 757–765 (1994).
17. P. Weibring, M. Andersson, H. Edner, and S. Svanberg, "Remote monitoring of industrial emissions by combination of lidar and plume velocity measurements, " Appl. Phys. B **66,** 383–388 (1998).
18. P. Weibring, Ch. Abrahamsson, M. Sjöholm, J. N. Smith, H. Edner, and S. Svanberg are preparing a manuscript titled "Multicomponent chemical analysis of gas mixtures using a continuously-tuneable lidar system.
19. K. V. Mardia and J. K. Kent, *Multivariate Analysis* (Academic, London, 1979).
20. K. Esbensen, *Multivariate Analysis*, 5th ed. (CAMO, Oslo, 2001).
21. A. S. Bangalore, R. A. Schaffer, G. W. Small, and M. A. Arnold, "Genetic algorithm-based method for selecting wavelength and model size for use with partial least-squares regression: application to near-infrared spectroscopy, " Anal. Chem. **68,** 4200–4212 (1996).
22. T. Lindström, U. Holst, P. Weibring, and H. Edner, "Analysis of lidar measurements using nonparametric kernel regression methods, " Appl. Phys. B **74,** 155–165 (2002).
23. H. Edner, G. W. Faris, A. Sunesson, and S. Svanberg, "Atmospheric atomic mercury monitoring using differential absorption lidar techniques, " Appl. Opt. **28,** 921–930 (1989).
24. H. Edner, P. Ragnarson, S. Svanberg, E. Wallinder, A. de Liso, R. Ferrara, and B. E. Maserti, "Differential absorption lidar mapping of atmospheric atomic mercury in Italian geothermal fields, " J. Geophys. Res. **97,** 3779–3786 (1992).
25. I. Wängberg, H. Edner, R. Ferrara, E. Zanzillotta, J. Munthe, J. Sommar, S. Svanberg, M. Sjöholm, and P. Weibring, "Mercury emissions from a chlor-alkali plant in Sweden, " Science Total Environ. (to be published).
26. P. Weibring, J. Swartling, H. Edner, S. Svanberg, T. Caltabiano, D. Condarelli, G. Cecchi, and L. Pantani, "Optical monitoring of volcanic sulfur dioxide emissions—comparison between four different remote-sensing spectroscopic techniques, " Optics Lasers Eng. **37,** 267–284 (2002).
27. D. Lognoli, C. Cecchi, L. Pantani, V. Raimondi, R. Chiari, Th. Johansson, P. Weibring, H. Edner, and S. Svanberg, "Fluorescence imaging of the Parma cathedral and baptistery, " Appl. Phys. B (to be published).
28. P. Weibring, "Environmental monitoring by multi-spectral lidar techniques, " Ph. D. dissertation, *Lund Reports on Atomic Physics*, LRAP-284 (Lund Institute of Technology, Lund, Sweden, 2002).